Applied Magnetic Resonance (2018) 49:1181–1199
https://doi.org/10.1007/s00723-018-1032-z

Applied
Magnetic Resonance

ORIGINAL PAPER

Characterization of the Lipid Binding Pocket in GM2AP and SapB with EPR Spectroscopy

Yong Ran[1] · **Gail E. Fanucci**[1]

Received: 26 April 2018 / Revised: 18 June 2018 / Published online: 24 July 2018

Abstract

Electron paramagnetic resonance (EPR) spectroscopy of spin-labeled lipids in complex with the sphingolipid activator proteins, GM2AP and SapB, was utilized to characterize the hydrophobic binding pocket of these lipid transfer proteins. Specifically, the EPR line shapes reveal that the mobility of the labeled lipids within the binding pockets of the transfer proteins are more restricted than when in a lipid bilayer environment and that lipids in GM2AP are slightly more restricted than in SapB. EPR accessibility based relaxation measurements show that the relative ratios of oxygen and water accessibility to sites along the acyl chains in lipids in complex with GM2AP are similar to the profiles obtained for a lipid bilayer albeit with lowered values. The results for SapB are quite different, with the oxygen profile mimicking a lipid bilayer, but there is a higher degree of water accessibility to the acyl chains in the SapB complex, likely because of the location of the lipid at the dimer interface in SapB coupled to dynamics of the dimer.

1 Introduction

Gangliosides are sialic-acid-containing glycosphingolipids (GSLs) that are part of the glycocalyx that covers eukaryotic cell surfaces, comprising a significant part of cell surface glycans in neuronal cells. Gangliosides have various biochemical and pathobiochemical functions [1–3]. Additionally, GSL catabolism is essential for normal cellular function, and numerous lysosomal storage diseases result when aberrations in GSL catabolism occur [4, 5]. The catabolism of GSLs with short oligosaccharide head groups and ceramide requires two proteins: a water-soluble lysosomal

Electronic supplementary material The online version of this article (https://doi.org/10.1007/s00723-018-1032-z) contains supplementary material, which is available to authorized users.

✉ Gail E. Fanucci
fanucci@chem.ufl.edu

[1] Department of Chemistry, University of Florida, PO BOX 117200, Gainesville, FL 32611-7200, USA

hydrolase and a small co-factor protein [4, 6, 7]. These co-factor proteins are a group of five lipid transfer proteins called the sphingolipid activator proteins, or SAPs [8]. The SAPs are predominantly water-soluble proteins that transiently interact with lipid vesicles under acidic conditions, where kinetics are regulated by lipid composition, charge and vesicle size [4, 7, 9–14]. In GSL catabolism, the SAPs function in the intra-lysosomal vesicles and extract their functional ganglioside ligand forming a water-soluble protein:lipid complex for reaction with a glycosidic hydrolase. Numerous lysosomal storage diseases can result from disruption of this catabolic cascade [5, 15, 16].

Of the five known SAPs, four of these, SapA, B, C and D, are proteolytically generated from a single prosaposin (PSAP) gene, bind to a variety of GSLs, are dimeric in structure, and have predominantly alpha-helical secondary structure [17–19]. The fifth of the SAPs, the GM2 activator protein (GM2AP), exists as a monomer in solution with a structure described as a beta-cup topology [20–24]. Lipid storage disorders can occur from mutations in the SAPs or GM2AP [4, 5, 15, 16].

Figure 1 shows ribbon diagrams of GM2AP and SapB that were crystallized with various phospholipids bound within their binding pockets. Although the SAPs have a primary function of ganglioside catabolism, both GM2AP and SapB can form complexes with phospholipids in addition to their ganglioside ligands [18–25] and have been implicated in functions related to immunity [26] and heart disease [27] and find uses in therapeutic strategies [25, 28–32]. Detailed analysis of various GM2AP X-ray structures reveals a rather large hydrophobic binding pocket capable of accommodating a variety of lipid ligands including lysolipids, detergents, phospholipids, and GM2 [21–24]. The orientation of GM2 differs from that of phospholipids bound to GM2AP. When phospholipids are bound (Fig. 1a) the phosphate group is located near the two putative membrane binding loops [23]. In contrast, when GM2 is modeled into the electron density, the ceramide tails pack nearer the helical loop region implicated in interacting with the hydrolase, whereas the GM2 head group is disordered and protruding outside of the hydrophobic binding pocket [24]. The crystal structure of SapB shows phosphatidylethanolamine, a lipid contaminant that occupies the protein's hydrophobic pocket throughout purification,

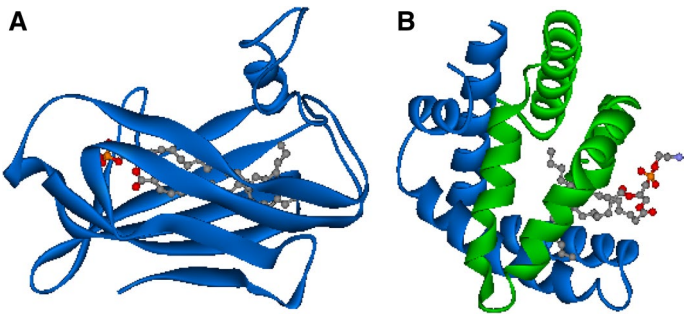

Fig. 1 Ribbon diagrams showing structures of **a** GM2AP with POPG bound (PDB ID 1PUB), **b** and SapB with POPE bound (PDB ID 1N69). In both structures the lipid molecules are rendered in ball and stick format

occupying a cleft between two monomers, with the lipid head group pointing in towards the protein interior (Fig. 1b). More recently, SapB has been crystallized in complex with chloroquine [30].

Here, we report the characterization of the physical environment of the lipid binding pocket of GM2AP and SapB by electron paramagnetic resonance (EPR) spectroscopy of spin-labeled lipid:protein complexes, with a series of *n*-doxyl phosphatidylcholine (*n*-PtdChol) and TEMPO-phosphatidylcholine (tempo-PtdChol) lipids (Fig. 2) as spin-probes. This method was previously applied to the phosphatidylinositol transfer protein Sec14p [33, 34]. We find for GM2AP and SapB, although the mobility of the lipids is similar in both proteins, the site-specific accessibility of nickel relaxation agents, and by inference, water to the lipids is higher in SapB than in GM2AP. Oxygen accessibility to GM2AP is also very low. Results also show that the mobility of the lipid is restricted in the protein:lipid complex when compared to a lipid bilayer. Protein:lipid complexes were prepared via the natural lipid extraction properties of these proteins, thus further demonstrating their ability to bind and extract non-ganglioside lipids in a pH dependent manner.

2 Methods

2.1 Materials

E. coli L-*α*-phosphatidylethanolamine (PE), 1-palmitoyl-2-oleoyl-*sn*-glycero-3-phospho(tempo)choline (tempo-PtdChol) and 1-acyl-2-(*n*-(4,4-dimethyloxazolidine-*N*-oxyl) stearoyl)-sn-glycero-3-phosphocholine (*n*-doxyl PtdChol) with the doxyl spin label positioned at $n = 5$, 7, 10, 12, 14, and 16 of the stearoyl chain were purchased from Avanti Polar Lipids (Alabaster, AL) as chloroform solutions. All lipids were used as received without further purification. Nickel (II) ethylenediamine-*N*,*N*-diacetic acid (NiEDDA) was prepared as described previously [35]. TLC plates were silica coated aluminum and were purchased from Whatman (Sanford, Maine). Unless otherwise stated, all other reagents were from Fisher Scientific (Pittsburg, PA) and used as received.

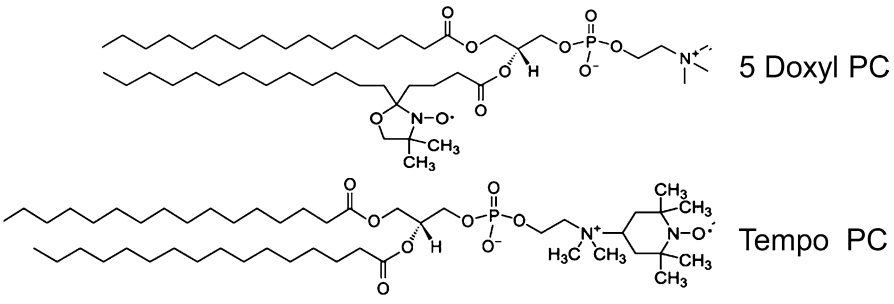

Fig. 2 Chemical structures of selected spin labeled phosphatidylcholine (SL-PtdChol)

2.2 Protein Expression and Purification

Recombinant human GM2AP was over expressed and purified as described previously following the methods of Wright [21–24]. Codon optimized DNA encoding SapB was synthesized by DNA2.0 Inc. (Menlo Park, CA). The DNA fragment was inserted into pET 16 b(+) multiple cloning sites between *Nco* I and *BamH* I. The resultant plasmid was transformed into Origami 2 (DE3) cells (Novagen, Germany). Expression and purification of SapB followed the method of Ahn with modification [18, 36]. Briefly, transformed Origami 2 (DE3) cells were grown at 37 °C to OD600 = 0.6 in 1 L of LB media containing 100 μg/mL ampicillin. Protein was over expressed by induction with isopropyl β-D-1-thiogalactopyranoside (IPTG) and cells were grown for an additional 6 h at 37 °C at 250 rpm. The cell pellets were collected and resuspended in lysis buffer (25 mM NaCl, 50 mM Tris HCl, pH 7.5) and lysed by passing through a French press (three times) and sonicating for 1 min. The lysates were clarified by centrifugation at 30,000*g* for 20 min and the supernatant was then heated to 85 °C in water bath for 10 min, followed by centrifugation at 30,000 g for 20 min. The supernatant was loaded to a 5 ml Q-Sepharose column (GE, Piscataway, NJ) pre-equilibrated in binding buffer (same as lysis buffer). After washing with 5 × volume of binding buffer, the protein was eluted with a linear gradient of elution buffer (1 M NaCl, 50 mM Tris HCl, pH 7.5). Fractions containing SapB were pooled and loaded onto a HiPrep 16/60 Sephacryl S-200 HR gel filtration column (GE) pre-equilibrated with 50 mM sodium acetate (NaOAc), pH 4.8. The purity of final protein samples were verified by SDS-PAGE gel. The structural integrity was verified by comparing circular dichroism spectra (Figure S1) with that reported for native SapB purified from porcine kidney [37] and recombinantly expressed SapB [25]. Sample homogeneity was also verified by HSQC NMR of ^{15}N labeled protein (Figure S2) and shows vast improvement over previously published NMR spectra for SapB [19]. Data were collected at the UF AMRIS facility and processed as described previously [38].

2.3 Preparation of Liposomes

Liposome dispersions of *n*-doxyl PtdChol and tempo-PtdChol were prepared by transferring the desired volume of lipid in chloroform into a glass vial, removing the organic solvent by a stream of nitrogen, and vacuum desiccating overnight to remove any residual solvent. For preparation of protein:lipid complexes, the dried lipid films were rehydrated in 50 mM NaOAc buffer, pH 4.8. To investigate effects of pH on extraction progression, lipid samples were also hydrated in 50 mM Tris pH 8.0 buffer as described previously [9]. For all samples, rehydration proceeded at room temperature followed by vortex mixing and three freeze–thaw cycles to ensure even distribution of the buffer. The stock lipid concentrations were 1 mM.

2.4 Formation of Protein:SL-PtdChol Complexes and Ligand Exchange Studies

Protein complexes of both GM2AP and SapB with spin-labeled phosphatidylcholine (SL-PtdChol) lipids proceeded by mixing ~ equimolar concentrations (1.2:1,

protein:lipid at 150 μM protein-dimmer for SapB) with preformed MLV dispersions at 22 °C. Nominally, lipid and protein samples were prepared in 50 mM NaOAc buffer, pH 4.8. For GM2AP at pH 4.8, complete sequestration of the lipids from the MLVs was completed in nearly 1 h. However, for SapB, this process took 8–12 h for completion, likely because the purified SapB protein contained phosphatidylethanolamine in the binding pocket [18]. For power saturation samples, an appropriate volume of stock NiEDDA solution was added to the protein:lipid complexes after complete solubilization of the liposome dispersions to give a final concentration of 50 mM (for GM2AP) and 12.5 mM or 25 mM (for SapB). NiEDDA concentration was verified by UV-VIS spectroscopy.

2.5 EPR Spectroscopy

CW X-band EPR spectra were obtained on either a modified Bruker ER200 spectrometer with an ER023M signal channel, an ER 032M field control unit or a Bruker E500 spectrometer equipped with a loop gap resonator (Medical Advances, Milwaukee, WI). The typical sample size for EPR measurements was 10 μL of ~ 150 μM SL-PtdChol:protein complex in NaOAc buffer, pH 4.8. Samples were loaded into 0.60 I.D × 0.84 O.D. capillary tubes. Sample temperature was maintained by passing nitrogen gas through copper coil submerged in a refrigerated bath (Thermo Scientific NESLAB RTE-7 digital one (− 25 to 150 °C ± 0.01) containing 40% ethylene glycol that then flowed to a quartz Dewar (Wilmad-Labglass) that surrounded the loop-gap resonator. Unless stated otherwise, cw-EPR experiments were performed at 22 ± 0.2 °C. For variable temperature experiments, the bath temperature was altered until the desired sample temperature was obtained. Sample temperature was measured by inserting an Omega temperature sensor and probe (OMEGA Engineering, Inc. Stamford, CT). All samples were allowed to equilibrate for 20 min. Typical temperature stability achievable with this set up is ± 0.1–0.2 °C [39, 40]. The spectral parameters for data collection were as follows: 2 mW microwave power; 100 kHz modulation frequency; 1.0–1.6 G modulation amplitude; 150 G magnetic field sweep; 40.6 s sweep time; and 16 ms detector time constant. When the time course of complex formation was monitored, single EPR scans were collected over the required time period. For end point spectra, typically 16 scans were signal averaged. Labview software was used for baseline correction and double integral area normalization. This software was generously provided by Drs. Christian Altenbach and Wayne Hubbell (UCLA).

2.6 Power Saturation EPR Spectroscopy

For power saturation experiments, samples (typically 7 μL) were placed into gas permeable TPX tubes (Medical Advances, Milwaukee WI), and saturation of the central resonance was monitored over microwave powers that varied from 0.2 to 63 mW. Power saturation data were collected on the Bruker ER200 spectrometer with a loop gap resonator. Three different data sets were collected for each SL-PtdChol:protein complex. The first data set was collected in a stream of nitrogen, the second in a stream

of air (20% oxygen). Compressed gas tanks were utilized during the experiments and the temperature was controlled by passing the gas through a copper coil submerged in a refrigeration bath. For the third data set, i.e., those containing NiEDDA, samples were purged with nitrogen gas prior to and during data collection. All data were collected at 22 ± 0.5 °C. Note, this temperature was easier for us to regulate with minor fluctuations than 25 °C.

2.7 Calculation of Line shape Parameters for motion Analyses

Due to the anisotropic nature of the g-tensor and A-tensor (hyperfine interaction) in nitroxide and doxyl spin-labels, motions within the nanosecond time regime modulate the X-band CW spectral line shape [41–46]. Here we utilize two different line shape analyses to characterize and compare motion of the SL-PtdChol lipids within the lipid:protein complexes. As the rate of spin-label motion increases and becomes more isotropic, line shapes narrow. The line width of the central X-band CW EPR spectrum reflects changes in motional averaging and becomes narrowed as motional rate and disorder increase. As such, the inverse of the peak-to-peak line width of the central resonance is commonly utilized as a mobility parameter defined as $M = (\Delta H_{pp})^{-1}$, where larger values indicate increased motional averaging. Spectra of doxyl-labelled lipids for sites within the acyl chains that experience restricted motion are broadened with additional spectral features that can be exploited to define an order parameter of motion, S, that is calculated by the following expressions:

$$S = \frac{T_{||} - T_{\perp}}{T_{zz} - T_{xx}} \left(\frac{a}{a'} \right) \tag{1}$$

$$a = {}^{1}/_{3}\left(T_{xx} + T_{yy} + T_{zz}\right) \tag{2}$$

$$a' = {}^{1}/_{3}\left(T_{||} + 2T_{\perp}\right) \tag{3}$$

where $T_{||}$ and $T_{\perp}$ are measured from the experimental spectra. $T_{zz} = 30.8$ G, $T_{xx} = T_{yy} = 5.8$ G, which have been determined from *N*-oxyl-4′,4′-dimethloxazolidine derivative of 5-a-cholestane-3-one, present as an impurity in single crystals of cholesteryl chloride and where a' accounts for differences in solution polarity effects [47–49].

2.8 Calculation of Collision Parameters from Power Saturation Measurements

The analysis used here follows that originally described by Altenbach [35, 50, 51]. For each of the three sample conditions, the values of $P_{1/2}$, which are related to the product $(T_{1e}T_{2e})^{-1}$, were determined by plotting the intensity of the central nitroxide resonance line, $A_{pp}(0)$, as a function of microwave power, P, and fitting with the following expression:

$$A_{\mathrm{pp}}(0) = I\sqrt{P}\left[1 + (2^{-\varepsilon} - 1)\frac{P}{P_{1/2}}\right]^{-\varepsilon} \tag{4}$$

where I is a scaling factor, $P_{1/2}$ is the power at which the resonance amplitude is one half its unsaturated value, and ε is a measure of the homogeneity of the resonance saturation. The relative accessibility of the paramagnetic species (either oxygen or NiEDDA) can be determined by the change in the values of $P_{1/2}$ under paramagnetic versus diamagnetic (nitrogen) conditions. The collision parameter, π, is related to the change in $T_{1\mathrm{e}}$ of the nitroxide and the frequency of collision with either NiEDDA or oxygen. Values for π are determined from the following expression:

$$\prod^{\mathrm{oxy}} \equiv \frac{\Delta P'_{1/2}(\mathrm{Oxy})}{P'_{1/2}(\mathrm{DPPH})} = \frac{P_{1/2}(\mathrm{Oxy})/\Delta H_{\mathrm{pp}}(\mathrm{Oxy}) - P_{1/2}(N_2)/\Delta H_{\mathrm{pp}}(\mathrm{N_2})}{P_{1/2}(\mathrm{DPPH})/\Delta H_{\mathrm{pp}}(\mathrm{DPPH})}, \tag{5}$$

where ΔH_{pp} is the peak-to-peak width (in Gauss) of the central transition line. Values for π with NiEDDA are determined analagously. DPPH is used to standardize resonators so values on different instruments and labs can readily be compared. For our resonator, the values of $P_{1/2}$ (DPPH) and ΔH_{pp} (DPPH)π were 11.4 ± 0.2 and 1.97 ± 0.02; respectively. π values for NiEDDA were calculated by substituting $P_{1/2}$ (NiEDDA) for $P_{1/2}$ (Oxy) in Eq. 2. When the power saturation method is utilized to determine the location of a spin-labeled site within a membrane bilayer, a depth parameter, Φ, is often defined. This value can be calculated by the following expression:

$$\Phi = \ln\left(\frac{\Delta P'_{1/2}(\mathrm{oxy})}{\Delta P'_{1/2}(\mathrm{NiEDDA})}\right). \tag{6}$$

Here, we use this same parameter to compare the local environment of the lipid within the binding pocket of the protein to that in the lipid bilayer. Our results for samples containing NiEDDA are reported as normalized values to 20 mM NiEDDA for comparison to work of others [52–56].

3 Results

3.1 Formation of SL-PtdChol:Protein Complexes

The formation of complexes between GM2AP and SapB with SL-PtdChol lipids was achieved by adding a slight excess of protein (1.2:1 P:L molar ratio) to preformed MLV dispersions of the target SL-PtdChol lipids. These proteins are known

to bind to, extract and transfer a variety of lipids and lipid-like molecules [18, 22, 23, 30, 57], where rates of extraction and transfer are modulated by lipid composition, charge and solution pH [4, 11, 14]. This lipid extraction ability was utilized to form SL-PtdChol lipid:protein complexes of both GM2AP and SapB where the SL-PtdChol was extracted from MLV dispersions. Figure 3 shows how the extraction process coupled to formation of the SL-PtdChol:protein complex can be observed via changes in the EPR spectra. The EPR spectra of all SL-PtdChol MLVs without addition of protein reveal a broad spectral component (~27 G peak-to-peak width) that results from exchange and dipolar interactions of the 100% spin-labeled lipid sample. Figure 3a shows the spectrum for 14-doxyl PtdChol MLVs in the absence of protein ($t=0$). Under acidic conditions that mimic the lysosome, 3 h after the addition of SapB, the spectrum becomes characteristic of a 14-doxyl-PtdChol molecule in a non-spin labeled lipid milieu overlain upon the broad background from the exchange broadened signal of the MLV. This finding can be explained by having spin-labeled lipid in two environments that are exchanging slowly. One of these environments is the binding pocket of the protein (which for a 1:1 complex would have no line shape broadening); the other is the MLV dispersions where the high concentration of spins leads to significant exchange broadening. After sufficient time has passed, the line shape becomes devoid of exchange broadening; indicating that nearly all of the lipid molecules have been extracted into the binding pockets of the proteins in a 1:1 complex (sample also becomes clear). Within the signal-to-noise ratio (SNR) of the EPR experiments, these results indicate that nearly all of the 14-doxyl PtdChol in the MLV dispersions have been sequestered by the proteins; thus forming 1:1 lipid:protein complexes.

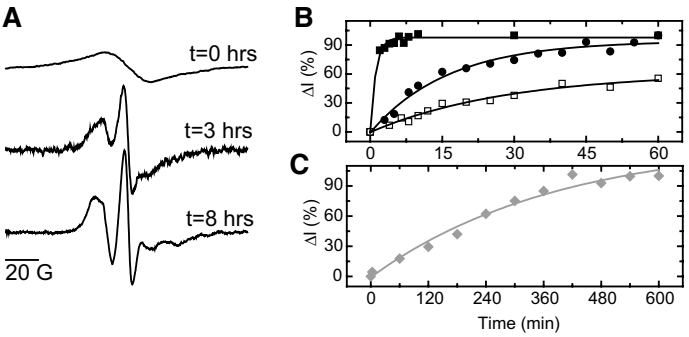

Fig. 3 EPR characterization of lipid:protein complexes. **a** 150 Gauss CW X-band EPR spectra of 14-Doxyl PtdChol as an MLV dispersion before addition of SapB ($t=0$), after incubation with slight excess of SapB for 3 and 8 h. Number of scans averaged were 36, 4 and 16; respectively. Samples were stored and data were collected at 22 °C. All samples were prepared in 50 mM NaOAc, pH 4.8. The time course of the formation of each protein-lipid complex was followed by monitoring the relative percentage change in normalized spectral intensity of the central resonance, $\Delta I\%$, defined as $100(I_{(t)} - I_o)/I_s$. The intensity of the last time points were set as I_s except data set collected at pH 6.4, for which the I_s of the data set at pH 4.8 was used. I_o is small and was approximated to be zero. **b** Complex formation as a function of time for GM2AP with tempo-PtdChol at pH 4.8 (solid circles), 14-doxyl PtdChol at pH 4.8 (solid squares) and at pH 6.4 (open squares). **c** Complex formation of SapB with 14-doxyl PtdChol at pH 4.8. The solid lines are fits with exponential functions

For all samples prepared here, the time course of the complex formation via lipid extraction proceeds over minutes to hours depending upon pH and is found to differ for GM2AP and SapB. Because the time course is on the minutes to hour time scale, the progression of the formation of the lipid:protein complex can be monitored by collecting EPR spectra and plotting the relative percentage change in the normalized intensity, ΔI (%), of the central resonance line as a function of time. This takes advantage of the fact that the spectral line shape becomes narrower, and hence, more intense, as the spin-exchange from the MLV dispersion is removed upon sequestration of the spin-labeled lipid into the lipid binding pocket of the protein. We are approximating the central line intensity to be proportional to the fraction of lipid in the lipid:protein complex because the intensity before addition of protein of the exchange broadened line at the position of the central transition can be approximated to zero. To ensure SL stability over time in the acidic solutions, the total lipid concentration of the resultant lipid:protein complex samples was determined by double integration of the resultant EPR spectrum and compared to a standard curve of 4-hydroxy TEMOPL. In all cases, spin-label concentration was $\sim 95 \pm 5\%$ of the original stock SL-lipid concentration used to form MLVs.

Using this approximation, we found that the data can be sufficiently fit with a single exponential (i.e., formation of the complex follows pseudo-first order kinetics) and the speed of complex formation can be modulated by pH. Example time course data sets for GM2AP with 14-doxyl PtdChol at pH 4.8 and pH 6.4 are shown in Fig. 3b. Within a few minutes, nearly complete extraction of spin-labeled lipid is achieved at pH 4.8 (solid squares) whereas the process is slowed as pH is increased (open squares). This result is expected given that SAPs are found in the acidic lysosome of cells and the pH dependence of lipid extraction and transfer of fluorescent lipids and fatty acids, as well as ganglioside degradation, have previously been documented [9–13, 15, 58–60]. The profile for complex formation for all of the *n*-doxyl PtdChol lipids are similar (data not shown), with relatively fast extraction at pH 4.8. The formation of tempo-PtdChol:GM2AP (solid circles) via extraction from MLVs is slower than that of the *n*-doxyl PtdChol lipids investigated here, but is completed within 3 h. Data for GM2AP with tempo-PtdChol are included in Fig. 3b for comparison.

In contrast, formation of all SL-PtdChol:SapB complexes proceeds much slower than observed for GM2AP; therefore, all SapB samples were allowed to react over night at room temperature for complete lipid solubilization to be achieved. The EPR results monitoring the formation of 14-doxyl PtdChol:SapB at pH 4.8 (solid squares) is shown in Fig. 3c. The quality of our *E.coli* expressed SapB was verified via CD and HSQC NMR spectroscopy (Figures S1 and S2; respectively). Therefore, we do not believe the slowness of this process reflects poor protein quality. However, the slower time course may reflect the presence of phosphatidylethanolamine (PE) in the binding pocket that is not readily removed during the purification procedure (PE is seen in TLC analysis of purified protein, data not shown); PE can also be seen in X-ray structures of SapB [18]. Another explanation for the apparent slowed complex formation is that SapB may contain more than one lipid in the pocket during

extraction [61]. Similar slow complex formation with SapB was observed independent of the type of lipid vesicles prepared (Figure S3).

Interestingly, the progression of complex formation amongst PE bound, dansyl-DHPE bound or unbound GM2AP are indistinguishable (Figure S3), perhaps indicating that for GM2AP the relative affinity for SL-PtdChol is greater than PE analogs or both lipids bind at the same time but in different pockets/orientations. Complex formation with SL-PtdChol when GM2AP was already bound to GM1 or GM2 gangliosides (i.e., GM1:GM2AP and GM2:GM2AP preformed complexes) proceeded slower than for unbound GM2AP, with doxyl-labeled lipids exchanging quicker than tempo-PtdChol (Figure S4). Overall, these results show that complexes can be formed by extraction of the SL-PtdChol lipids from liposomes and provide evidence that the time course of extraction/complex formation of spin-labeled phospholipids from neutral vesicles at pH 4.8 is slower for SapB than for GM2AP.

3.2 Local Lipid Dynamics in the Protein Binding Pocket

Some of the earliest characterizations of the gradient in acyl-chain mobility in lipid bilayers came from analysis of the EPR spectral line shapes of *n*-doxyl fatty acids incorporated into liposomes and cellular membranes [47, 62–65]. The relative mobility of the spin-label is reflected by the linewidth of the central transition, ΔH_{pp}, of the doxyl/nitroxide X-band CW spectrum (Fig. 4a). Another parameter utilized to describe the anisotropic motion of doxyl spin-labels in lipid environments is the order parameter, $\boldsymbol{S}$, which is determined by measuring various spectra feature (Fig. 4b, c) and Eqs. 1, 2, 3 where a value of 1 is indicative of "frozen" rigid-limit spectra, and where $\boldsymbol{S} = 0$ indicates more isotropic motion. Here, various SL-PtdChol lipids were used to characterize the lipid dynamics in the hydrophobic binding pockets of GM2AP and SapB. Figure 5a shows a stack plot of EPR spectra for each SL-PtdChol:protein complex. Figure 5b reports the inverse mobility parameter $(\Delta H_{pp})^{-1}$. In general, for both GM2AP and SapB the

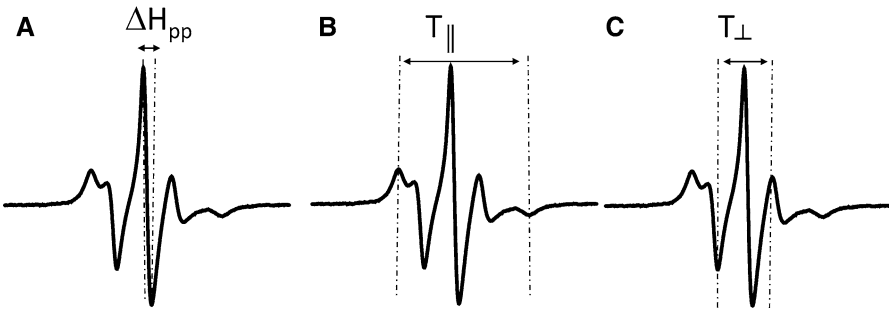

Fig. 4 Illustrative X-band CW EPR spectra showing how mobility line shape parameters are measured from spectra. **a** The central line width, $\Delta \boldsymbol{H}_{pp}$ and the parallel (**b**) and perpendicular (**c**) tensor components utilized to determine the order parameter, $\boldsymbol{S}$. All parameters are reported in units of Gauss (*G*)

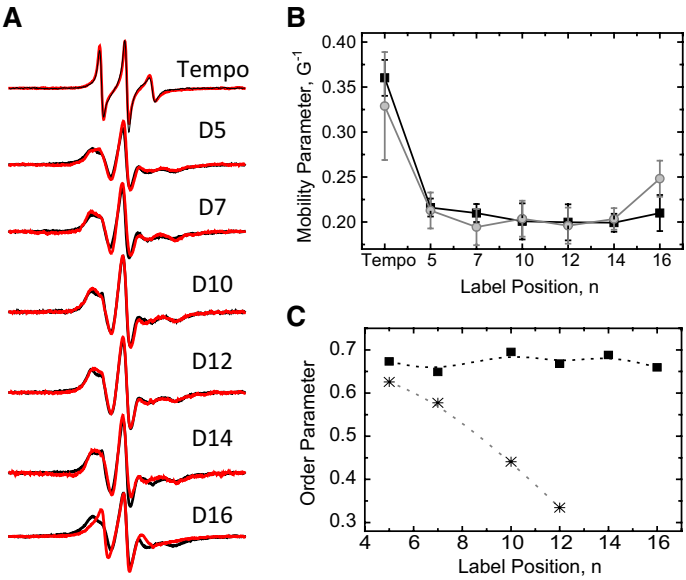

Fig. 5 **a** Stack plot of 150 Gauss CW X-band EPR spectra of *n*-doxyl and tempo-PtdChol with GM2AP (black) and SapB (red) at 22 °C. Each set is vertically offset and plotted with equal intensities of the central resonance line for ease of comparison of changes in breadth (and hence mobility) if observed. Corresponding line shape parameters of **b** mobility (ΔH_{pp}^{-1}) and **c** order parameter, $\boldsymbol{S}$, are plotted. Data for GM2AP are plotted as solid circles. Data for SapB are reported with open grey circles. Asterisks represent values for DOPC bilayers. Error bars were obtained from three separate measurements of the same sample on different days and are most affected by fluctuations in temperature stability

mobility of each SL-PtdChol is similar at all positions except D16, which displays higher mobility in SapB. Additionally, the mobility of the doxyl-moiety for positions $n = 5$ to 14 is relatively invariant and more restricted than for SL-PtdChol in lipid bilayers. As expected from crystal structures, the mobility of tempo-PtdChol is high and similar to what is found in a lipid bilayer. Figure 5c plots values of the order parameter, $\boldsymbol{S}$, [49] determined from the spectra of the GM2AP lipid complexes and SL-PtdChol in DOPC (DOPC spectra shown in Figure S5). For all cases, SL-PtdChol in the protein-lipid complexes at each site is more restricted than in the bilayer, especially for sites $n = 10$ to 16 and the lipid within the protein pocket does not show the typical mobility gradient when in a lipid bilayer environment [40, 47].

3.3 Temperature Effects on Spin Label Mobility in SL-PtdChol SapB and GM2AP Complexes

The EPR line shapes for *n*-doxyl PtdChol lipids in GM2AP and SapB reveal a high degree of structural rigidity. Variable temperature experiments provide a means of interrogating the effective energy barrier required for lipid movement within the pocket. Figure 6a shows stack plots of EPR spectra for several

SL-PtdChol:GM2AP complexes over the temperature range of 9–28 °C. As the temperature is increased, the EPR spectrum narrows and becomes more intense, indicating the lipid is experiencing increased motion. From the slopes of Arrhenius type plots (Figure S6) relative differences in the energy barrier for lipid mobility within GM2AP and SapB can be seen. Figure 6b compares the slope values obtained via this effective Arrhenius analysis for several SL-PtdChol lipids in GM2AP and SapB. In general, results show a trend of an increasing energy barrier to motion of the spin probe as the position moves from the head group to the end of the acyl chain. For most sites, there is also a slightly higher barrier to label mobility in GM2AP than in SapB.

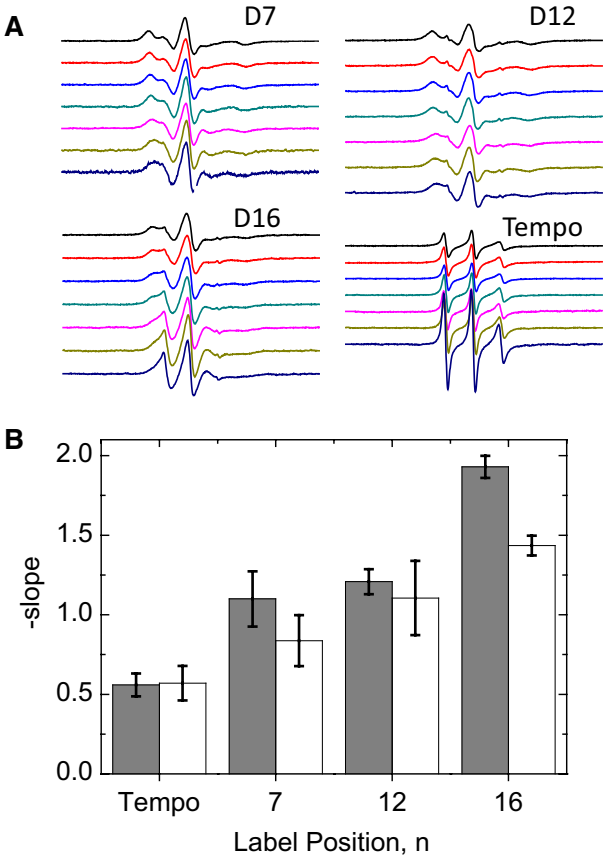

Fig. 6 **a** Stack plots of 150 G CW EPR spectra of 7-doxyl, 12-doxyl, 16-doxyl and tempo- PtdChol GM2AP complexes over the temperature range of 9–28 °C in 3° increments (top to bottom). Spectra are integral area normalized and vertically offset for clarity. **b** Graphical representation of the slope values obtained from Arrhenius type plots of $\ln(\Delta H_{pp}^{-1})$ versus $1/T$ for GM2AP (grey bars) and SapB (open bars) complexes. The value of the slope is proportional to the energy barrier for lipid mobility in the pocket. Error bars represent the 95% confidence limit in the value of the slope obtained from linear regression analysis

3.4 Local Accessibility of Lipids in the Protein Binding Pocket

The local accessibility of a nitroxide spin label to paramagnetic colliders provides information that can be used to investigate protein docking at bilayer interfaces [9, 53, 66–70], protein folding and assembly [71–73], and membrane protein structure and conformational changes [43, 55, 74–78]. Although pulsed EPR methods provide a more direct experimental approach of measuring changes in the nitroxide spin–lattice relaxation lifetime [33, 79]; the power saturation method is a robust and relatively easy way to obtain accessibility information without the need for specialized pulsed EPR instrumentation [35, 50]. Previously, the accessibility of the soluble paramagnetic nickel complex, NiEDDA, to the Sec14p lipid transfer protein was characterized by pulsed EPR relaxation measurements [33]. Here, the accessibility of NiEDDA to each of the SL-PtdChol lipids in complex with either GM2AP or SapB was investigated by CW power saturation experiments. The local accessibility gradient of a spin label to oxygen, which is preferentially soluble in the hydrophobic interior of the lipid bilayer, and to a water-soluble metal-complex can be utilized to determine the 'depth' of the spin-label along the bilayer normal [54, 71, 80]. The depth parameter, Φ, is often utilized to determine the location of a spin label on a membrane protein within the lipid bilayer and compared to values obtained from *n*-doxyl PtdChol lipids used calibration curves. Here we utilize the same parameter, which shows the relative accessibility of each spin-labeled site to both oxygen and NiEDDA. With NiEDDA concentrations normalized to 20 mM and oxygen supplied from air tanks at typical atmospheric pressures, values of Φ approach −3 indicating location in bulk water, values of Φ of ~ 0 indicate a location near the bilayer interface (equal collisions with oxygen and Ni complex), and values approaching +3 are indicative of an environment similar to that deep within a bilayer interior [43, 53, 54, 56, 80]. The limiting values of Φ are impacted by the identity of the Ni complex (i.e., NiAA versus NiEDDA) and concentration, as well as the oxygen concentrations and temperature, as the relaxation mechanism is dominated by collisions [70]. Hence, care must be taken when comparing actual values of Φ across experiments. Our values reported here have been normalized to 20 mM NiEDDA for this comparison.

Figure 7a plots values of Φ obtained for each SL-PtdChol in complex with either GM2AP or SapB. For GM2AP, the trend in the Φ parameter follows that expected for *n*-doxyl PtdChol lipids when incorporated into a membrane bilayer [43, 56, 80]. The tempo-PtdChol lipid bound with GM2AP has very high accessibility to NiEDDA whereas 5-doxyl PtdChol has a Φ value near zero. As the position of the spin label moves incrementally along the acyl-chain, the value of the depth parameter becomes more positive, indicating a higher accessibility to oxygen than to the aqueous metal complex. The Φ parameter value at site 16 is similar to that of site 7, possibly indicating protrusion from the pocket, similar to how the 16-doxyl lipid is stated to "snorkel" to the bilayer interface because of the hydrophilic nature of the tail termini [81]. This trend of relative accessibility to polar and non-polar paramagnetic mimics that of the lipid bilayer.

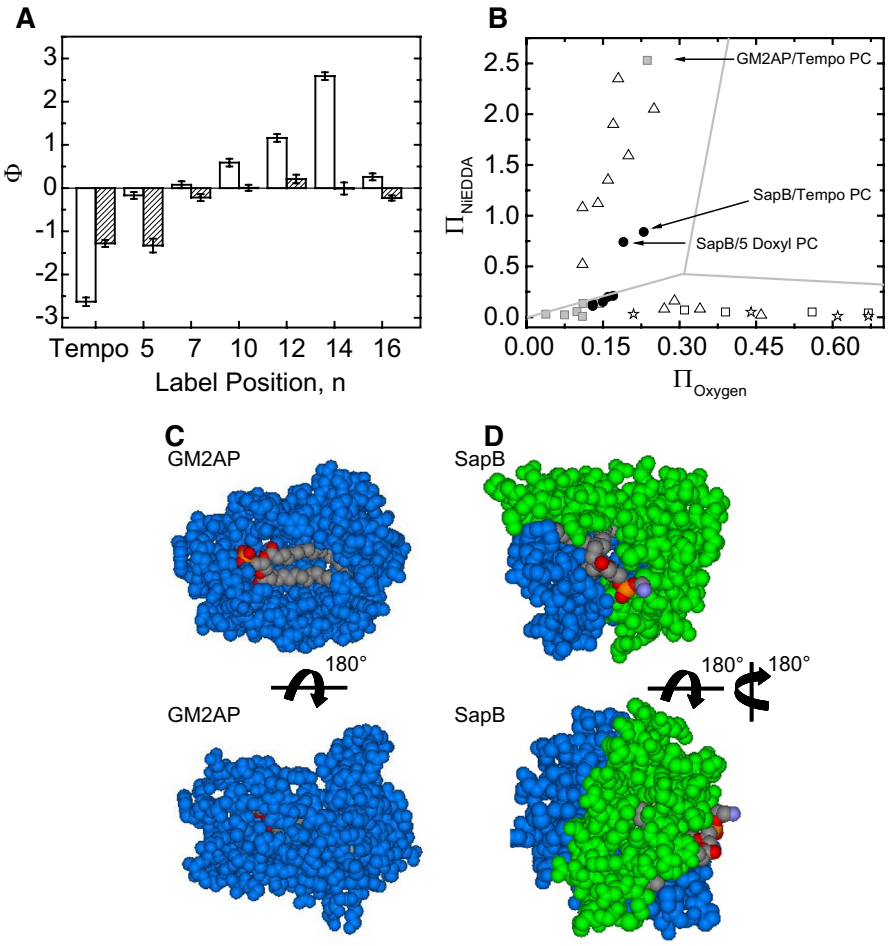

Fig. 7 Power saturation results of *n*-doxyl and tempo- PtdChol with GM2AP and SapB. **a** Φ values for GM2AP complexes (blank) and SapB complexes (hash lines). Error bars were determined from triplicate measurements on the same sample. Final NiEDDA concentrations were 50 mM for GM2AP with *n*-doxyl PtdChol, 12.5 mM for SapB with 5-doxyl and tempo-PtdChol and were 25 mM for other lipids with SapB. $P'_{1/2}$ values used in the mathematical calculation of Φ were arithmetically scaled to 20 mM which normalizes results to an effective concentration of 20 mM so that Φ values can be compared and discussed in terms of observations seen within lipid bilayers and other membrane protein systems. **b** Plots of collision parameter, Π, of GM2AP (solid squares) and SapB (solid circles) complexes with *n*-doxyl and tempo-PtdChol. The Π values for spin-labeled sites of the C2 domain of cPLA2 bound to PC:PS bilayers (3:1) (open triangles), of bacteriorhodopsin (open stars) and of *n*-doxyl labeled lipids (open squares) (about 1 mol% in PC:PS = 3:1, room temperature) are plotted for comparison. Data for C2 domains, bacteriorhodopsin and lipids are taken from Refs. [54, 56, 82]; respectively. Data shown for GM2AP and SapB are normalized results for 20 mM NiEDDA concentrations. The solid lines are guides determined empirically for membrane bound and aqueous exposed sites in proteins. Space fill representation of **c** GM2AP (PDBID:1PUB) and **d** SapB (PDBID:1N69) showing a front (top) and back (bottom) view of the crystallized protein-lipid complexes. In each case, the lipid molecules are rendered in different colors to show the relative accessibility of each site to solvent

In contrast, however; for all *n*-doxyl acyl chain positions along the PtdChol lipid in complex with SapB, near zero or negative values of Φ are obtained. Results indicate that the oxygen accessibility at SL-PtdChol in SapB is slightly higher than the equivalent site in in GM2AP, but where the NiEDDA accessibility is also higher. In fact, experimentally to collect data, concentrations of NiEDDA were lowered for samples of SapB (12. 5 and 25 mM versus 50 mM) compared to GM2AP. This finding may be explained by the dimeric nature of SapB and perhaps more time average fluctuations of water accessibility to the lipid tails. Collision parameters, π, for oxygen and NiEDDA are graphically depicted in Fig. 7b. This empirical phase diagram is constructed by plotting values of π given in the literature for sites in bacteriorhodopsin [56], KcsA [82], and the C2A domain of synaptotagmin [54] as well as for *n*-doxyl lipids in membrane bilayers [54]. Typically, sites that are within the bilayer have low accessibility to NiEDDA with high accessibility to oxygen. Sites that are in the bulk aqueous solvent or are solvent exposed have the opposite trend. Accessibility of both oxygen and NiEDDA are very low in GM2AP (solid grey squares), which may not be expected based upon the apparent exposure in the crystal structure (Fig. 7c). Most sites for the lipids in SapB (solid circles) have higher accessibility to oxygen than those in GM2AP (solid squares). However, the accessibility of the NiEDDA to the *n*-doxyl PtdChol in SapB (solid circles) is also much higher than in GM2AP or even a bilayer environment. Perhaps dynamics of the dimeric SapB protein with the lipid in the interface allows for greater water penetration than would again be expected from the space filling model of the crystal structure (Fig. 7d).

4 Discussion

4.1 Dynamics in GM2AP and SapB May Modulate Solvent Exposure to the Lipid Binding Pocket

Figure 7c, d show space filling models of GM2AP:PG and SapB:PE complexes determined from X-ray crystallography. Results from EPR power saturation measurements (π values) show that for GM2AP in solution, the accessibility of the acyl-chains to aqueous soluble NiEDDA is lower than expected from the degree of exposure of the acyl chains in the GM2AP:PG crystallographic complex, indicating that the protein dynamics may cause the loops to close around the lipid when in solution [83]. In fact, π_{NiEDDA} values are comparable to those for membrane embedded sites in bacteriorhodopsin (stars in Fig. 6b). On the other hand, values for π_{O2} for GM2AP are substantially lower than those observed for spin labelled lipids within a lipid environment or membrane embedded sites on bateriorhodopsin. In SapB, the lipid binding "pocket" is formed within the dimer interface and shows a high degree of exposure of the PE head group with the acyl-chains burred within the interface with little solvent exposure. In agreement, the π_{NiEDDA} values for both tempo- and 5-doxyl PtdChol:SapB are similar to those seen for the membrane associated C2 domain. However, values of π_{O2} for both tempo- and 5-doxyl PtdChol:SapB are also higher than expected for aqueous exposure. Perhaps SapB closes around the lipid, or that oxygen penetrates more readily into the pocket than within a lipid bilayer.

For sites 7-16 in SL-PtdChol:SapB complexes, π_{NiEDDA} values are higher than those seen in GM2AP, membrane bound sites in bR and lipid bilayers. Again, this finding is surprising based upon the static crystal structure, indicating that protein dynamics in solution may allow more water penetration to the interior of the lipid binding pocket [18].

Although the documented function of SAPs is in stimulating ganglioside catabolism within the lysosomal compartment of cells [1, 6–8, 15], this work shows that SAPB and GM2AP can readily extract and bind and phospholipids. These findings and work of others suggests that other functional roles of SAPs may revolve around their ability to transfer and bind phospholipids in other cellular locations [25, 28–32, 61]. Clearly both GM2AP and SapB not only form relatively stable complexes with the SL-PtdChol molecules, but both proteins are capable of extracting these ligands from lipid bilayer dispersions without anionic lipids or the unique endosomal lipid bis(monoacylglycero)phosphate; albeit with slower times [11].

4.2 Use of Spin-Labels in Characterizing Protein:Lipid Interactions

Spin-labeled lipids have received extensive usage in studies that characterize the dynamics and lipid packing arrangements in various lipid bilayers [47, 62–65, 81], and these spin-probes have also been extensively utilized to study lipid-protein interactions of either integral membrane proteins or surface associated membrane proteins [84–92]. Here, we show how SL-lipids can provide valuable information not only about the local environment within the lipid binding pocket, but also provide indirect evidence regarding relative affinity and lipid transfer ability. To date, we have not been able to form GM2AP or SapB lipid complexes with phospholipids containing fluorescent probes on the fatty acid chains, indirectly showing that the smaller doxyl spin-probe can be more readily accommodated within the hydrophobic lipid binding sites. Furthermore, although GM2AP will extract dansyl-DHPE from neutral vesicles [58], SapB does not. Yet, SapB does form a complex when dansyl-DHPE is added from ethanolic solution (data not shown) and will extract and form a complex with the tempo-head group-labeled lipid and when tempo-PC is presented from lipid dispersions. Although spin-probes (and fluorescent tags) are larger and likely more perturbing than a radioactive labeled lipid, detailed information about the physical and chemical environment can be gleaned from analysis of various spectroscopic properties of spin-labeled lipid ligands and the EPR methods described within should be applicable to a wide range of lipid binding and lipid transfer proteins with an appropriately spin-labeled ligand analog. Perhaps the SL-PtdChol:protein complexes can be exploited to assay the relative affinity of these proteins for various lipid ligands as has been performed by other methods [13, 57, 61], providing valuable information comparable to that from studies where fluorescent probes were utilized to modify various lipid-ligands of lipid transfer proteins [13, 58, 93–97].

5 Conclusions

The environment of the lipid binding pocket and mobility of lipids bound to two SAPs, namely GM2AP and SapB, were characterized via EPR spectroscopy of protein in complex with spin-labeled phospholipids. The lipid:protein complexes were prepared by allowing the proteins to extract the ligands from lipid dispersions. This process was slow, occurring over minutes to hours, and spectra were collected during the time course of the lipid extraction and complex formation. EPR line shapes of the bound lipids, in both GM2AP and SapB, reveal that the lipids in the proteins are more restricted in their mobility than when in lipid bilayers, and the lipids in GM2AP are found to be more restricted than those in SapB. EPR power saturation studies show that the lipids in SapB have a higher degree of water accessibility, likely resulting from the location of the binding site residing at the dimeric interface. Results surprisingly show that both GM2 and GM1 can be displaced by the spin-labeled lipids in GM2AP. These findings, taken together with our previous studies, indicate that GM2AP and SapB have an affinity for phospholipids that readily competes with gangliosides and we speculate that the molecular basis behind this finding is that the lipid head group size increases in non-polar character (dansyl > tempo), and the affinity for those glycerophospholipids decreases.

Acknowledgements This work was supported by the National Institutes of Health Grants GM077232 and S10RR031603. A portion of this work was performed in the McKnight Brain Institute at the National High Magnetic Field Laboratory's AMRIS Facility, which is supported by National Science Foundation Cooperative Agreement No. DMR-1157490 and the State of Florida.

References

1. K. Sandhoff, T. Kolter, Trends Cell Biol. **6**, 98–103 (1996)
2. T. Kolter, ISRN Biochem. **2012**, 506160 (2012)
3. R.L. Schnaar, R. Gerardy-Schahn, H. Hildebrandt, Physiol. Rev. **94**, 461–518 (2014)
4. K. Sandhoff, Biochimie **130**, 146–151 (2016)
5. C.R. Ferreira, W.A. Gahl, Transl. Sci. Rare Dis. **2**, 1–71 (2017)
6. W. Furst, K. Sandhoff, Biochim. Biophys. Acta **1126**, 1–16 (1992)
7. T. Kolter, F. Winau, U.E. Schaible, M. Leippe, K. Sandhoff, J. Biol. Chem. **280**, 41125–41128 (2005)
8. T. Kolter, K. Sandhoff, Annu. Rev. Cell Dev. Biol. **21**, 81–103 (2005)
9. J.D. Mathias, Y. Ran, J.D. Carter, G.E. Fanucci, Biophys. J. **97**, 1436–1444 (2009)
10. Y. Ran, G.E. Fanucci, Biophys. J. **97**, 257–266 (2009)
11. N. Remmel, S. Locatelli-Hoops, B. Breiden, G. Schwarzmann, K. Sandhoff, FEBS J. **274**, 3405–3420 (2007)
12. G. Schwarzmann, M. Wendeler, K. Sandhoff, Glycobiology **15**, 1302–1311 (2005)
13. N. Smiljanic-Georgijev, B. Rigat, B. Xie, W. Wang, D.J. Mahuran, Biochim. Biophys. Acta **1339**, 192–202 (1997)
14. S. Locatelli-Hoops, N. Remmel, R. Klingenstein, B. Breiden, M. Rossocha, M. Schoeniger, C. Koenigs, W. Saenger, K. Sandhoff, J. Biol. Chem. **281**, 32451–32460 (2006)
15. T. Kolter, K. Sandhoff, Biochim. Biophys. Acta **1758**, 2057–2079 (2006)
16. L. Kuchar, J. Ledvinova, M. Hrebicek, H. Myskova, L. Dvorakova, L. Berna, P. Chrastina, B. Asfaw, M. Elleder, M. Petermoller, H. Mayrhofer, M. Staudt, I. Krageloh-Mann, B.C. Paton, K. Harzer, Am. J. Med. Genet. A **149A**, 613–621 (2009)

17. J.S. O'Brien, K.A. Kretz, N. Dewji, D.A. Wenger, F. Esch, A.L. Fluharty, Science **241**, 1098–1101 (1988)
18. V.E. Ahn, K.F. Faull, J.P. Whitelegge, A.L. Fluharty, G.G. Prive, Proc. Natl. Acad. Sci. USA **100**, 38–43 (2003)
19. M. John, M. Wendeler, M. Heller, K. Sandhoff, H. Kessler, Biochemistry **45**, 5206–5216 (2006)
20. D.J. Mahuran, Biochim. Biophys. Acta **1393**, 1–18 (1998)
21. C.S. Wright, S.C. Li, F. Rastinejad, J. Mol. Biol. **304**, 411–422 (2000)
22. C.S. Wright, L.Z. Mi, S. Lee, F. Rastinejad, Biochemistry **44**, 13510–13521 (2005)
23. C.S. Wright, L.Z. Mi, F. Rastinejad, J. Mol. Biol. **342**, 585–592 (2004)
24. C.S. Wright, Q. Zhao, F. Rastinejad, J. Mol. Biol. **331**, 951–964 (2003)
25. D.D. Dixson, V.Y. Yu, R.P. Doyle, Anal. Biochem. **419**, 145–152 (2011)
26. A. Darmoise, P. Maschmeyer, F. Winau, Adv. Immunol. **105**, 25–62 (2010)
27. B. Rigat, H. Yeger, D. Shehnaz, D. Mahuran, Biochem. Biophys. Res. Commun. **385**, 576–580 (2009)
28. J. Wojton, Z. Chu, H. Mathsyaraja, W.H. Meisen, N. Denton, C.H. Kwon, L.M. Chow, M. Palascak, R. Franco, T. Bourdeau, S. Thornton, M.C. Ostrowski, B. Kaur, X. Qi, Mol. Ther. **21**, 1517–1525 (2013)
29. H.W. Davis, N. Hussain, X. Qi, Mol. Cancer **15**, 33 (2016)
30. B.P. Huta, M.R. Mehlenbacher, Y. Nie, X. Lai, C. Zubieta, F. Bou-Abdallah, R.P. Doyle, Chem. Med. Chem. **11**, 277–282 (2015)
31. J. Tinklepaugh, B.M. Smith, Y. Nie, K. Moody, K. Grohn, F. Bou-Abdallah, R.P. Doyle, Chem. Photo. Chem. **1**, 256–259 (2017)
32. W. Xu, J. Yuan, S. Yang, C.B. Ching, J. Liu, ACS Synth. Biol. **5**, 1404–1411 (2016)
33. T.I. Smirnova, T.G. Chadwick, R. MacArthur, O. Poluektov, L. Song, M.M. Ryan, G. Schaaf, V.A. Bankaitis, J. Biol. Chem. **281**, 34897–34908 (2006)
34. T.I. Smirnova, T.G. Chadwick, M.A. Voinov, O. Poluektov, J. van Tol, A. Ozarowski, G. Schaaf, M.M. Ryan, V.A. Bankaitis, Biophys. J. **92**, 3686–3695 (2007)
35. C. Altenbach, D.A. Greenhalgh, H.G. Khorana, W.L. Hubbell, Proc. Natl. Acad. Sci. USA **91**, 1667–1671 (1994)
36. V.E. Ahn, K.F. Faull, J.P. Whitelegge, J. Higginson, A.L. Fluharty, G.G. Prive, Protein Expr. Purif. **27**, 186–193 (2003)
37. A.J. Waring, Y. Chen, K.F. Faull, R. Stevens, M.A. Sherman, A.L. Fluharty, Mol. Genet. Metab. **63**, 14–25 (1998)
38. X. Huang, I.M. de Vera, A.M. Veloro, M.E. Blackburn, J.L. Kear, J.D. Carter, J.R. Rocca, C. Simmerling, B.M. Dunn, G.E. Fanucci, J. Phys. Chem. B **116**, 14235–14244 (2012)
39. T.E. Frederick, P.C. Goff, C.E. Mair, R.S. Farver, J.R. Long, G.E. Fanucci, Chem. Phys. Lipids **163**, 703–711 (2010)
40. T.E. Frederick, J.N. Chebukati, C.E. Mair, P.C. Goff, G.E. Fanucci, Biophys. J. **96**, 1847–1855 (2009)
41. W.L. Hubbell, D.S. Cafiso, C. Altenbach, Nat. Struct. Biol. **7**, 735–739 (2000)
42. L. Columbus, W.L. Hubbell, Trends Biochem. Sci. **27**, 288–295 (2002)
43. G.E. Fanucci, D.S. Cafiso, Curr. Opin. Struct. Biol. **16**, 644–653 (2006)
44. R.P. Mason, J.H. Freed, J. Phys. Chem. **78**, 1321–1323 (1974)
45. D.E. Budil, S. Lee, S. Saxena, J.H. Freed, J. Magn. Reson. **120**, 155–189 (1996)
46. J.P. Barnes, Z. Liang, H.S. McHaourab, J.H. Freed, W.L. Hubbell, Biophys. J. **76**, 3298–3306 (1999)
47. W.L. Hubbell, H.M. McConnell, J. Am. Chem. Soc. **93**, 314–326 (1971)
48. J.R. Trudell, E.N. Cohen, W.L. Hubbell, Ann. N. Y. Acad. Sci. **222**, 530–538 (1973)
49. K. Schorn, D. Marsh, Spectrochim. Acta Part A Mol. Biomol. Spectrosc. **53**, 2235–2240 (1997)
50. C. Altenbach, W. Froncisz, R. Hemker, H. McHaourab, W.L. Hubbell, Biophys. J. **89**, 2103–2112 (2005)
51. C. Altenbach, T. Marti, H.G. Khorana, W.L. Hubbell, Science **248**, 1088–1092 (1990)
52. E. Rufener, A.A. Frazier, C.M. Wieser, A. Hinderliter, D.S. Cafiso, Biochemistry **44**, 18–28 (2005)
53. A.A. Frazier, C.R. Roller, J.J. Havelka, A. Hinderliter, D.S. Cafiso, Biochemistry **42**, 96–105 (2003)
54. A.A. Frazier, M.A. Wisner, N.J. Malmberg, K.G. Victor, G.E. Fanucci, E.A. Nalefski, J.J. Falke, D.S. Cafiso, Biochemistry **41**, 6282–6292 (2002)
55. W.L. Hubbell, C. Altenbach, C.M. Hubbell, H.G. Khorana, Adv. Protein Chem. **63**, 243–290 (2003)
56. W.L. Hubbell, C. Altenbach, Curr. Opin. Struct. Biol. **4**, 566–573 (1994)

57. C.B. Fluharty, J. Johnson, J. Whitelegge, K.F. Faull, A.L. Fluharty, J. Neurosci. Res. **63**, 82–89 (2001)
58. Y. Ran, G.E. Fanucci, Anal. Biochem. **382**, 132–134 (2008)
59. S.C. Li, Y. Hama, Y.T. Li, Methods Enzymol. **363**, 230–241 (2003)
60. A. Vogel, G. Schwarzmann, K. Sandhoff, Eur. J. Biochem. **200**, 591–597 (1991)
61. J. Tinklepaugh, B.M. Smith, E. Hanlon, C. Zubieta, F. Bou-Abdallah, R.P. Doyle, ACS Omega **2**, 7141–7145 (2017)
62. W.L. Hubbell, H.M. McConnell, Proc. Natl. Acad. Sci. USA **64**, 20–27 (1969)
63. S. Rottem, W.L. Hubbell, L. Hayflick, H.M. McConnell, Biochim. Biophys. Acta **219**, 104–113 (1970)
64. B.M. Sefton, B.J. Gaffney, J. Mol. Biol. **90**, 343–358 (1974)
65. J.B. Gaffney, Proc. Natl. Acad. Sci. USA **72**, 664–668 (1975)
66. D.Z. Herrick, W. Kuo, H. Huang, C.D. Schwieters, J.F. Ellena, D.S. Cafiso, J. Mol. Biol. **390**, 913–923 (2009)
67. W. Kuo, D.Z. Herrick, J.F. Ellena, D.S. Cafiso, J. Mol. Biol. **387**, 284–294 (2009)
68. Y. Lin, R. Nielsen, D. Murray, W.L. Hubbell, C. Mailer, B.H. Robinson, M.H. Gelb, Science **279**, 1925–1929 (1998)
69. A. Gross, W.L. Hubbell, Biochemistry **41**, 1123–1128 (2002)
70. A.L. Turner, O. Braide, F.D. Mills, G.E. Fanucci, J.R. Long, Biochim. Biophys. Acta **1838**, 3212–3219 (2014)
71. W.L. Hubbell, A. Gross, R. Langen, M.A. Lietzow, Curr. Opin. Struct. Biol. **8**, 649–656 (1998)
72. R. Langen, J.M. Isas, W.L. Hubbell, H.T. Haigler, Proc. Natl. Acad. Sci. USA **95**, 14060–14065 (1998)
73. R. Langen, J.M. Isas, H. Luecke, H.T. Haigler, W.L. Hubbell, J. Biol. Chem. **273**, 22453–22457 (1998)
74. E. Perozo, D.M. Cortes, P. Sompornpisut, A. Kloda, B. Martinac, Nature **418**, 942–948 (2002)
75. E. Perozo, A. Kloda, D.M. Cortes, B. Martinac, Nat. Struct. Biol. **9**, 696–703 (2002)
76. P. Zou, H.S. McHaourab, J. Mol. Biol. **393**, 574–585 (2009)
77. H.A. Koteiche, S. Chiu, R.L. Majdoch, P.L. Stewart, H.S. McHaourab, Structure **13**, 1165–1171 (2005)
78. M.A. Do Cao, S. Crouzy, M. Kim, M. Becchi, D.S. Cafiso, A. Di Pietro, J.M. Jault, Protein Sci. **18**, 1507–1520 (2009)
79. R.D. Nielsen, S. Canaan, J.A. Gladden, M.H. Gelb, C. Mailer, B.H. Robinson, J. Magn. Reson. **169**, 129–163 (2004)
80. G.E. Fanucci, N. Cadieux, C.A. Piedmont, R.J. Kadner, D.S. Cafiso, Biochemistry **41**, 11543–11551 (2002)
81. B. Dzikovski, D. Tipikin, J. Freed, J. Phys. Chem. B **116**, 6694–6706 (2012)
82. E. Perozo, D.M. Cortes, L.G. Cuello, Nat. Struct. Biol. **5**, 459–469 (1998)
83. J.D. Carter, J.D. Mathias, E.F. Gomez, Y. Ran, F. Xu, L. Galiano, N.Q. Tran, P.W. D'Amore, C.S. Wright, D.K. Chakravorty, G.E. Fanucci, J. Phys. Chem. B **118**, 10607–10617 (2014)
84. P.F. Knowles, A. Watts, D. Marsh, Biochemistry **20**, 5888–5894 (1981)
85. D. Marsh, A. Watts, R.D. Pates, R. Uhl, P.F. Knowles, M. Esmann, Biophys. J. **37**, 265–274 (1982)
86. A. Watts, I.D. Volotovski, R. Pates, D. Marsh, Biophys. J. **37**, 94–95 (1982)
87. M. Esmann, D. Marsh, Biochemistry **24**, 3572–3578 (1985)
88. G.L. Powell, P.F. Knowles, D. Marsh, Biochim. Biophys. Acta **816**, 191–194 (1985)
89. H. Gorrissen, D. Marsh, A. Rietveld, B. de Kruijff, Biochemistry **25**, 2904–2910 (1986)
90. M. Esmann, K. Hideg, D. Marsh, Biochemistry **27**, 3913–3917 (1988)
91. L.E. Bretscher, A.H. Buchaklian, C.S. Klug, Anal. Biochem. **382**, 129–131 (2008)
92. M.E. Rauch, C.G. Ferguson, G.D. Prestwich, D.S. Cafiso, J. Biol. Chem. **277**, 14068–14076 (2002)
93. P. Nava, M. Cecchini, S. Chirico, H. Gordon, S. Morley, D. Manor, J. Atkinson, Bioorg. Med. Chem. **14**, 3721–3736 (2006)
94. S. Morley, V. Cross, M. Cecchini, P. Nava, J. Atkinson, D. Manor, Biochemistry **45**, 1075–1081 (2006)
95. J.K. Atkinson, P. Nava, G. Frahm, V. Curtis, D. Manor, Ann. N. Y. Acad. Sci. **1031**, 324–327 (2004)
96. W.X. Zhang, G. Frahm, S. Morley, D. Manor, J. Atkinson, Lipids **44**, 631–641 (2009)
97. C.S. Rao, T. Chung, H.M. Pike, R.E. Brown, Biophys. J. **89**, 4017–4028 (2005)